PETROGRAPHIC STUDY ON THE POTENTIAL ALKALI-REACTIVITY OF FERRO-NICKEL SLAGS FOR CONCRETE AGGREGATES

Tetsuya Katayama
Cement/Concrete Research Laboratory, Sumitomo Cement Co.,Ltd.
585 Toyotomi, Funabashi, Japan 274

In order to assess the potential alkali-reactivity of ferro-nickel slags produced in Japan, petrographic examinations have been made, based on norm calculations, mode determination, XRD and EPMA analyses of mineral phases contained in slags. It was revealed that the alkali-reactivity of these slags is mostly negligible. In the low-calcium molten slags (CaO<1%), silica is enriched up to SiO_2 60-65% in the residual melt through crystallization of olivine during cooling, but the glass with this range of silica is usually innactive. It may show exceptional alkali-silica reactivity, only in the case of poorly quenched slag, which has a very fine spinifex texture composed of dendritic olivine and fine glass matrix. In contrast, in high-calcium slag (CaO>5%), silica enrichment does not occur during cooling (SiO_2 <56%), which explains its low reactivity.

1. INTRODUCTION

Ferro-nickel slags are some of the potential sources for concrete aggregates in Japan. They consist mainly of SiO_2 and MgO, and are divided into two categories, i.e. high-calcium slag (CaO>5%), made during the sintering process by adding limestone flux, and low-calcium slags (CaO<1%), produced by melting the raw materials at high temperatures. (Table 1). The former is (A) semi-crystalline, water-cooled slag, while the latter contains three types, (B) spherical and semi-crystalline, air-granulated slag, (C) well-crystalline, air-cooled slag, and (D) glassy, water-granulated slag (Table 1).

Although only a few species of these slags have been known to have potential alkali-reactivity (Yamamoto and Akiyama(1)), the nature of the reactivity has not yet been fully understood, like natural aggregates. Hence to clarify this aspect, a detailed and comprehensive petrographic study was made of these slags to try and relate the mineral compositions to their reactivity. The usefulness of petrography in assessing the potential reactivity of these slags, particularly by means of identifying the nature of the glass phases contained in them, will be discussed in this paper.

2. MINERAL COMPOSITIONS OF FERRO-NICKEL SLAGS

A total of 30 samples of ferro-nickel slags were offered to the author, including four currently produced types (A,B,C,D) of both average run and selected samples (Committee, Japan Mining Industry Association (3)), as well as their old counterparts tested and equipped with reactivity data by previous researchers ((1), Yoda (2)), along with some not currently produced types for reference (E,F (1)). Petrographic examinations were made of these samples to identify potentially reactive materials, based on norm calculations from bulk chemical analyses (Table 2), mode determination of minerals by microscopy (Table 3), phase identification by XRD analyses, and quantitative analyses by EPMA of both crystalline and glass phases. A selected result out of 1100 EPMA measurements (Katayama (4)) of these samples is given in Table 4.

2.1 Normative Compositions

Calculation of slightly modified CIPW norms indicates that the ferro-nickel slags contain more than 70% normative pyroxenes, mostly enstatite, and corresponding mineralogically pyroxenites (Table 2). Because nickel ores, originated from weathered serpentinites after peridotites, have a higer silica/magnesia ratio than the original rocks due to magnesium leaching during weathering, the slags produced from the ores attain 50% SiO_2, which chemically resembles pyroxenites rather than the original peridotites. All the slags are undersaturated with silica, and normative olivine is calculated instead of normative quartz. This suggests that, unlike volcanic rocks, they have little possibility in producing reactive silica minerals, such as cristobalite and tridymite. High calcium-slags contain much normative diopside. There is a correspondence between normative and modal compositions in the well-crystallized slag, but is lacking where the slag is glassy. No modal counterpart of normative anorthite was found.

2.2 Crystal Phases of Ferro-Nickel Slags

Under the microscope, some of the molten slags (B, C) resemble, in appearance, stony meteorite and komatiite, consisting of radially crystallized enstatite and olivine with surrounding glass, while sintered slag (A) resembles a volcanic rock boninite, consisting of enstatite phenocrysts and interstitial glass. In the ferro-nickel slags, the dominant phase enstatite occurs as three modifications, i.e. protoenstatite, clinoenstatite and orthoenstatite: the former two occur in the low-calcium slags (B, C, D), while the last one occurs with augite and pigeonite in the high-calcium slag (A). During cooling of molten slags, olivine crystallizes first, followed by pxroxenes.

Olivine. Olivine occurs in the molten slags as forsterite, as has been reported (Kawahara et al. (5)). In the glassy part of the slags, particularly water-granulated slag (D), forsterite forms dendritic to elongate crystals, arranged parallelly or radially in a glass matrix (Figure 3). This resembles the spinifex texture of komatiite, an ultramafic rock formed by rapid cooling of melt of ultramafic magma (MacKenzie et al. (6)). This texture is also visible in some of the air-granulated slag and a glassy surface layer of air-cooled slag. Forsterite forms granular microphenocrysts in the slowly cooled slag. In the water-cooled slag (A), olivine occurs as small grains of a pale yellowish color, having crysolite composition with fayalite component (fa) 12-13%.

Protoenstatite. This phase is found in the rapidly cooled portion of low-calcium, molten slags. It is only stable at high temperatures and no terrestrial counterpart has been reported. In thin section, it is a transparent crystal showing straight extinction. In the air-cooled slag (C), it is formed in a transitional zone between the surface layer and the annealed interior of the slag, in radial arrangement nearly perpendicular to the slag surface, surrounded by a glass matrix. Well-developed crystals have cracks perpendicular to its c-axis, and often partly inverted to clinoenstatite with multiple twinning. In the spherical grains of air-granulated slag (B), protoenstatite occurs as radiating crystals pseudomorphic to radial olivine (Figure 3), resembling the texture of chondrule in a stony meteorite. It may be also present as cryptocrystalline to ill-shaped mosaics in the devitrified glass, which can be identified by XRD by its simple lines.

Clinoenstatite. This is the dominant phase of the air-cooled slag (C). It is formed through inversion from protoenstatite during cooling, but retains the original radial texture of this mineral in the transitional zone. In the annealed interior of the slag, clinoenstatite develops large elongate crystals of light-green color, with up to 4cm in length, forming parallel bundles. Under the microscope, it is fractured due to volume changes that occurred during the inversion. Clinoenstatite has polysynthetic twining parallelly developed on the (100) plain with extinction angles of 25-27°, whose optical property closely resembles the clinoenstatite phenocrysts reported from a high-magnesian andesite of Papua (Dallwitz et al. (7)). This phase is easily identified also by XRD analysis by its multiple refrection lines. EPMA analysis revealed that both proto- and clinoenstatite have nearly the same compositions resembling pure enstatite, with a low wollastonite component (Wo) 0.1% and a low ferrosilite composition (Fs) 4%.

Orthoenstatite. This constituent is the dominant pyroxene in the water-cooled slag (A). It occurs as rectangular phenocrysts to microphenocrysts, up to 0.6mmm, resembling in shape orthopyroxenes in the volcanic rocks. It is a transparent crystal without cracks, but is sometimes concentrically zoned with minute inclusions entrapped during the process of crystal growth. It is formed at higher temperatures than other pyroxenes in this slag. Orthoenstatite forms a continuous series of solid solution, with Fs ranging from 2-10%, with fixed Wo at 3-4% (Figure 1). It contains higher calcium than the protoenstatite and clinoenstatite in the low-calcium slags. The increase in Fs component of the solid-solution suggests a gradual decrease in temperature occurred during its crystallization. Though peak patterns of XRD resemble other phases of enstatite, it can be identified using a characteristic reflection at 2θ Cu$k\alpha$ = 33.1° (d= 2.702 A, (421)).

Pigeonite. This is strictly a magnesian pigeonite, whose terrestrial counterpart has not been reported. This phase is stable only at high temperatures and preserved when quickly cooled. In the slag A, it occurs in a small quantity (1%) as rectangular microphenocrysts (0.1mm) with a pale yellowish tint, or as thin rims to orthoenstatite, or as large phenocrysts (0.3-0.5mm) having exsolution lamellae developed on the crystal plain parallel to the (100) plane. The microphenocrysts constitute a continuous series of solid solution from Fs 2-10% at a fixed level of Wo at 6-7% (Figure 1). An increase in Fs component suggests gradual lowering of temperature during formation of this phase.

Augite. This mineral constitutes a minor phase (5%) in the slag A. It is mostly a subcalcic augite having compositions intermediate between pigeonite and augite. Typical augite occurs as isolated small grains in the groundmass, having a petal-like shape of a pale yellow to yellowish brown tint, or rarely, as exsolution lamellae in the large pigeonite phenocryst. The groundmass augite is the latest product of crystallization from the residual melt at low temperatures. Subcalcic augite occurs as thin rims (2μ in thickness) surrounding orthoenstatite and pigeonite, which constitutes a continuous series of solid solution from a magnesian pigeonite (En82, Fs11, Wo7) to an augite (En52, Fs15, Wo33)(Figure 1). Subcalcic augite is generally thought to be an unstable phase, and its occurrence has been attributed to disequilibrium fractional crystallization of the melt during quick cooling (Kushiro et al.(8)). This condition partly holds with this slag. But some part of the interior of the slag are slowly cooled, where pigeonite phenocrysts decompose and exsolve into enstatite and augite along their (100) plane.

Cristobalite. Although this is a disequilibrium phase in the ferro-nickel slags, a trace of this mineral was detected only by XRD in some of air-granulated slag (B). This may be the result of fractional crystallization of melt during cooling.

2.3 Glass Phases of Ferro-Nickel Slags

The glass phases in the ferro-nickel slags differ greatly in their content depending on their production method, particularly the cooling rate. Their content ranges from 80-90% in the water-granulated slag (D), 40-50% in the air-cooled slag (B), 20-30% in the water-cooled slag (A), to less than 5% in the air-cooled slag (C)(Table 3). A reference water-granulated slag sample (F) contained 99% glass. In this paper, glasses occurring in these molten slags were classified into five categories, based on the glass-mineral assemblages: quenched glass, semi-quenched glass, medium glass, annealed glass, and devitrified glass in cooling order. A close correlation is assumed between experimentaly determined cooling rates (Matsuo et al.(9)) and each type of glass (Table 5).

The composition of the glass also changes considerably during crystallization of a melt. In high-calcium sintered slag (A), calcium is enriched in the residual melt to form augite while silica is not in this process (Table 4, Figure 1). In this slag, olivine and enstatite, formed during sintering, may be embedded within a quenched glass by quick cooling, or may be subsequently interspersed with a small amount of pigeonite in a semi-quenched glass, or with subcalcic augite to augite in medium to annealed glasses. In contrast, in the low-calcium molten slags (B, C, D), which contain about 20% of normative olivine, silica is enriched in the residual melt during olivine crystallization (Table 4, Figure 2). The glasses in the low-calcium molten slags are described as follows:

Quenched glass. This glass, uniformly colorless and transparent in thin section, carries no crystals. It is formed by rapid chilling of molten slag from high temperatures, before olivine starts to crystallize. Since no differentiation of crystal phases has started, it has the same composition as that of the bulk chemistry of the slag (Figure 2). Comparing the silica content of D, B, F to that of bulk, the following was observed: D, SiO_2 52% vs. 51%, B, 53% vs. 52%, and F, 52-55% vs. 54% (Tables 1, 4). In the granulated slags (B, D), fine grains of slag, originally molten droplets, are highly vitrified to fix bulk compositions of slags. Some of the grains of air-granulated slag (B) have oxidized skin of quenched glass on their surface (thickness 0.1mm), while the inner part is somewhat differentiated. A referential slag (F) consists solely of this glass (Table 3). The quenched glasses have low silica and, as discussed later, are less alkali-reactive.

Semi-quenched glass. This glass, fine-grained, contains only olivine as a crystalline phase and characterizes the early stage of differentiation of melt (Figures 1, 2). It is formed through insufficient quenching (semi-quenching) of molten slag from high temperatures, which permits rapid crystallization of olivine as the primary crystal in the slag melt. This glass dominates the glassy water-granulated slag (D), but may occur in air-granulated slag (B), and in a surface layer of air-cooled slag (C)(Tables 3, 4). It constitutes a fine-grained, spinifex texture in which oriented crystals of elongate olivine are embedded in a glass matrix (Figure 3). In granulated slags, differentiation of melt proceeds in larger grains owing to poor efficiency of quenching. In thin section, this glass in smaller grains is pale yellowish, while larger grains, enriched in silica, show yellowish brown or darker color. The surface area of this glass, bordered between the glass and olivine, is larger among glasses in the ferro-nickel slags.

Semi-quenched glass is always more siliceous than the bulk chemistry of the slag, with up to about 10% more silica, whose maximum SiO_2 ranging from 60% (slag D) to 64% (slag C) (Table 4). In the MgO-SiO_2 system, which approximates the low-calcium molten slags, equilibrium crystallization of olivine from a melt produces a slightly silica-rich residual melt, because this mineral is less siliceous (SiO_2 40%) than the bulk composition of the slags (average SiO_2 52%). However, disequilibrium crystallization of olivine would cause more intensive enrichment of silica, e.g. composition of slag D moves across the protoenstatite field into the cristobalite field during cooling (Figure 2). This produces extremely silica-rich residual melt, along with an excess amount of olivine in a disequilibrium state, while minerals other than olivine are not formed. Similar process has been reported in the artificial chondrules (Tsuchiyama et al.(10)), where the residual glass, containing only olivine, is enriched up to 14% more than the original melt whose SiO_2 is 55%, comparable to the ferro-nickel slag. As shown later, such silica-rich glass with fine texture is considered to be alkali-reactive.

Medium glass. This glass appears in association with newly forming pyroxene along with residual olivine, and characterizes the middle stage of differentiation of melt (Figure 2). It is formed through intermediate cooling of molten slag, through which excess olivine reacts with residual melt peritectically to produce protoenstatite at moderate temperatures. The glass bears a brownish tint, and is accompanied by protoenstatite and/or clinoenstatite. It dominates the air-granulated slag (B)(Figure 3), as well as the transitional zone beneath the surface layer of air-cooled slag (C)(Table 3).

In the cross section of air-cooled slag (C, particularly C_T), a complete sequence of cooling can be seen from the semi-quenched surface layer (< 4mm in depth), through the moderately cooled transitional zone (4-8mm), to the slowly cooled interior (> 8-12mm) (Figure 2, Table 3). The glass content in these zones does not change continuously, but rather discretely. In the transitional zone where protoenstatite is formed rapidly, the content of surrounding melt appears nearly constant throughout the zone. However, a compositional inhomogenity is observed in the medium glass, i.e. silica content of this glass in the air-granulated slag (B) fluctuates between 58-65% even in a small distance ($<10\mu$) within the same grain. Such difference tends to be larger in larger grains (Table 4). This is the result of fractional crystallization of isolated residual melt, enclosed between interstices of growing pyroxene crystals. This process crystallizes a trace of disequilibrium mineral cristobalite from a slica-rich melt, now present as medium glass.

Annealed glass. This glass, usually colorless, is found in a small quantity (< 3%) in the annealed portions of air-cooled slag (C) whose texture is apparently holocrystalline. It represents a residual melt of the late stage of differentiation of slag melt, i.e. the composition of the melt, after crystallizing all the normative enstatite and whereby depleting magnesium, moves out from the cristobalite field and slightly decreases the silica content to less than 60% (Figures 1, 2, Table 4). During cooling, alkalies are enriched up to 100 times the original slag (Na_2O 1%, K_2O 0.4%). Similarly, aluminum and calcium are concentrated up to 8 times in this glass, producing 30% of normative anorthite but its modal counterpart was not found. The trend of this differentiation of melt resembles a hypothetical process of partial melting of peridotites in the upper mantle, which has been believed to produce magmas of igneous rocks in the earth's crust.

Devitrified glass. This contains a cryptocrystalline to ill-shaped mosaic of enstatite, likely protoenstatite, that has been crystallized from a quenched glass during annealing at relatively low temperatures. It is found in a small amount in air-granulated slag.

3. POTENTIAL REACTIVITY AND DISCUSSIONS

Comparisons were made between the results of petrographic analyses and alkali-reactivity tests of ferro-nickel slags, to identify the mineral species that show potential reactivity. Reactivity data came from the Committee (3), tested according to the JIS A 5308 chemical and mortar bar tests (A, B, C, D), except for a selected (B_S, (11)) or referential older samples (E, F, (1), (2)). Chemical test results are shown in Figure 4.

3.1 Potential Reactivity of Slag

Ferro-nickel slags tend to test as deleterious in the chemical test, while they have negligible expansivity in the mortar bar test, except for the slag D. According to Tomosawa and Yokoyama (12), the dissolved silica (Sc) in the past years ranged from about 50-60 mmol/l for slag A, 40-150 mmo/l for slag B, 40-140 mmol/l for slag C, and 160-230 mmol/l for slag D. There is a linear relationship between the value of Sc and the expansion in the mortar bar test (12, Kobayashi et al. (13)), but even older samples of the slag A, B, C with each maximum Sc, produced small expansion (less than 0.04% /6 months, (12)), while the slag D caused deleterious expansion even with a minimum Sc (3).

Water-cooled slag. Sample A, containing interstitial glasses with low slica content (SiO_2 < 56%), is on the borderline between the innocuous and the deleterious fields in the chemical test, and shows little expansion (3). This slag does not contain reactive glass.

Water-granulated slag. Sample D, dominated by fine-grained semi-quenched glass, presented a maximum Sc among ferro-nickel slags examined (3), and the most deleterious expansion in the mortar bar test. This slag does not show a pessimum phenomenon (3, 12), but its deleterious expansion can be effectively supressed by an addition of ground granulated blastfurnace slag (3, 12) or fly ash (Nagataki (14)). The reactivity of this slag is solely attributable to the semi-quenched glass, because reactive cristobalite was not detected. This is supported by a finding that this slag, when reheated to 1100°C (1) or 1250°C (9) and subjected to a devitrification of this glass phase, showed little expansion in the mortar bar test (1), or a decrease in Sc into an innocuous level (9). The abundance of this glass probably determines the reactivity of the slag. Because a reference sample (E), containing much more quenched glass than D, was marginally to deleteriously expansive (S6 of (1), 2), while sample (F), consisting of quenched glass, produced a minimum Sc and little expansion (S5' of (1)).

Air-granulated slag. Sample B, dominated by intermediate glass with a trace of cristobalite, fell into the deleterious field near the border in the chemical test, while the mortar bar test proved its innocuousness (3). However, when this slag contains a greater amount of semi-quenched glass (about 20%) instead of cristobalite, it tends to present a higher Sc (B_S), suggesting that this glass is responsible for the potential alkali-reactivity of the slag.

Air-cooled slag. Sample C, located on the border line in the chemical test, is innocuous in the mortar bar test (3). However, only a glassy layer formed on the surface of this slag may produce a high Sc and deleterious expansion (Kusuda et al.(15)). Since this layer mainly consists of semi-quenched glass and lacks silica minerals, this glass is assumed to be the source of potential reactivity of this slag.

3.2 Potential Reactivity of Interstitial Glasses

It is clear from the foregoing that the reactive material in the low-calcium molten slags, is fine-grained, semi-quenched glass. Since the composition of this glass ranges from SiO_2 52% to 65%, nearly andesitic to dacitic relative to silica, it is necessary to determine at what composition this glass produces potential alkali-reactivity, as well as the factors such as the content and texture.

Composition of Reactive Glass. Katayama et al.(16) revealed that the silica content of natural and artificial glasses, uniquivocally determines their alkali reactivity in the chemical test. They noted a linear relationship between the log of Sc and the content of silica in the glass, and considered the glass with more than SiO_2 65% as potentially reactive (Figure 5). The result directly applies to the quenched glass of a completely glassy slag (F :S5' of (1)), where the low content of SiO_2 (54%) in this glass explains its low Sc and innocuous nature. However, when the glass has a fine texture, reactivity becomes more intense than predicted: water-granulated slag (D), containing fine-grained semi-quenched glass, is estimated to have Sc less than 50 mmol/l from its silica content of glass (SiO_2 60%), whereas measured Sc exceeds 220 mmol/l (3), several times larger. Such discrepancy is due to the large surface area of this glass. Thus, in the ferro-nickel slags, SiO_2 60% in the glass could be the critical value for producing alkali-silica reactivity. This explains the low reactivity of the high-calcium slag (A), because this slag contains low-silica glass with less than SiO_2 56%.

Content of Reactive Glass. A simple chemical calculation, using bulk chemical data of slag and the glass content determined by microscopy along with EPMA compositions of glass, suggests that the following mineral composition is possible for slag D: 20 wt% of olivine (SiO_2 40%, based on EPMA analysis) and 80 wt% of glasses (average SiO_2 55%); the glass part is also chemically equivalent to the combination of 20 wt% of silica-rich, semi-quenched glass (SiO_2 60%), plus 50 wt% of intermediate semi-quenched glass (SiO_2 55%), plus 10 wt% of low-silica quenched glass (SiO_2 52%). This means that the silica-rich semi-quenched glass, contained in a rather small amount (20%), could be the cause of alkali-reactivity of this slag. In contrast, neither medium nor annealed glasses, although they contain up to 65% silica, are considered as particularly reactive because their occurrence is rather limited and the surface area is smaller than the former glass. The presence of the potentially reactive glass in the ferro-nickel slags also explains their lack of pessimum phenomenon, since reactive natural glass, such as dacitic glass with SiO_2 65% in andesite (16), have no pessimum.

Thus, the petrographic examination identifies the presence of a potentially reactive glass phase in the ferro-nickel slags, and explains the nature of their alkali-reactivity. This approach will be useful not only for users of these slag aggregates in assessing their potential reactivity, but also for slag producers to feed back information on the cooling conditions to produce good aggregates for concrete.

4. CONCLUDING REMARKS

1. Ferro-nickel slags are generally innocuous aggregate, despite the variety of their chemistry and production method. However, they may present exceptional alkali-silica reactivity only in the case that the slag, when poorly quenched, has a very fine spinifex texture composed of slender olivine and semi-quenched glass.

2. Semi-quenched glass, containing enriched SiO_2 up to 60-65%, is practically the sole reactive phase in the slags. It has no pessimum phenomenon. Silica enrichment in this

glass occurs in the low-calcium molten slags (CaO<1%), due to rapid disequilibrium crystallization of olivine from a melt. In contrast, in the high-calcium slag (CaO>5%), it does not occur and this explains the lack of reactivity of this slag.

3. The formation of the reactive glass could be supressed, either by controling the cooling rate of molten slags, such as rapid quenching, moderate or slow cooling, or by reheating to devitrify the glass, or by an addition of calcium into the slag system. More research will be needed to confirm the most effective process to supress the reactivity.

5. ACKNOWLEDGEMENTS

This study is part of a work performed at the Committee of Japan Mining Industry Association, chaired by Professor S. Nagataki, Tokyo Institute of Technology, and vice-chaired by Professor F. Tomosawa, University of Tokyo. The author is grateful to the association for providing the data on reactivity and bulk chemical analysis of samples. Associate Professor Y. Yamamoto, Tsukuba University, and Professor A. Yoda, Ashikaga Institute of Technology, provided the author with referencial slag samples. EPMA anaysis was done at the Ocean Research Institute, University of Tokyo, with the help by Dr. T. Ishii.

6. SYMBOLS USED

d = spacing of crystal lattice (A = Angstrom, 10^{-8}cm)
En = molar ratio of enstatite component, $MgSiO_3$, in the pyroxene solid solution
Fs = molar ratio of ferrosilite component, $FeSiO_3$, in the pyroxene solid solution
μ = micron (10^{-4}cm)
Rc = reduced alkalinity (mili mole/litter)
Sc = dissolved silica (mili mole/litter)
Wo = molar ratio of wollastonite component, $CaMgSi_2O_6$, in the pyroxene solid solution

7. REFERENCES

1. Yamamoto, Y., and Akiyama, A., 1986, Proc. 7th I.C.A.A.R., Ottawa, 496.
2. Yoda, A., 1985, "Mortar Bar Test of Ferro-Nickel Slags", Report, Committee, Ferro-Nickel Slag, Architectural Institute of Japan, 12p. (* in Japanese)
3. Committee on Ferro-Nickel Slag, 1991, Japan Mining Industry Association (JMIA)
4. Katayama, T., 1991, "Petrograhy of Ferro-Nickel Slags", Report, Committee on the Ferro-Nickel Slag, JMIA, 139p. (*).
5. Kawahara, M., Yokoo, M., Kajiyama, K., Shirane, Y., and Yanagase, T., 1984, Nihon Kogyo Kyokaishi, 100, 435. (*)
6. MacKenzie, W.S., Donaldson, C.H., and Guilford, C., 1984, "Atlas of Igneous Rocks and their Textures", see p.84, Longman, Essex, England.
7. Dallwitz, W.B., Green, D.H., and Thompson, J.E., 1966, J.Petrology 7, 375.
8. Kushiro, I., Nakamura, Y., Kitayama, K., and Akimoto, S., 1971, Proc. 2nd Lunar Science Conference 1, 481.
9. Matsuo, Y., Takebe, H., Ota, Y., and Morinaga, K., 1989, Shigen Sozai Gakkaishi, 105, 1067. (*)
10. Tsuchiyama, A., Nagahara, H., and Kushiro, I., 1980, Proc. 5th Symp. on Antarctic Meteorites, Mem. Nat. Inst. Polar Res. Spec. Issue, 17, 83.
11. Tamura, H., Takahashi, T., and Nishimori, K., 1991, "Concrete Bar Test of Ferro-Nickel Slags", Report, Committee, Ferro-Nickel Slag, JMIA, 21p. (*)
12. Tomosawa, F., and Yokoyama, M., 1992, Proc. 9th I.C.A.A.R., London. (This Conference).
13. Kobayashi, M., Kaga, H., Yokoyama, M., and Sugiyama, T., 1989, Proc. 11th. Annual Meeting, Japan Concrete Institute, 111. (*)
14. Nagataki, S., 1991, "Supressing Effect of Fly Ashes against AAR Expansion of Ferro-Nickel Slags", Report, Committee, Ferro-Nickel Slag, JMIA. (*)
15. Kusuda, H., Nishiyama, T., Hirai, H., Murai, K., and Nabeya, H., 1990, Proc. Shigen Sozai Gakkai, Autumun Meeting, D., 5. (*)
16. Katayama, T., StJohn, D.A., and Futagawa, T., 1989, Proc. 8th I.C.A.A.R., Kyoto, 537.

TABLE 1 - Chemical Compositions of Ferro-Nickel Slags

Slag	A	B	C	D	E*	F*
Type	W/Cl	A/Gr	A/Cl	W/Gr	W/Gr	W/Gr
	sinter R.K.	melt E.F.	melt E.F.	melt E.F.	melt E.F.	melt B.F.
SiO_2	53.0	51.6	53.5	51.2	54.2	54.0
Al_2O_3	2.3	2.2	2.2	1.7	1.2	3.2
Cr_2O_3	1.2	1.3	1.1	1.2	0.7	0.6
FeO**	9.1	7.1	3.7	9.8	6.4	3.9
NiO	0.4	0.1	0.1	0.1	0.1	0.2
MgO	28.8	35.3	37.6	34.2	37.0	26.0
CaO	4.8	1.6	1.3	0.4	0.2	11.2
Na_2O		tr	tr			0.2
K_2O		0.0	0.0			tr
Total	99.6	99.2	99.5	98.6	99.8	99.3

E*, F* = currently not produced
W/Cl = water-cooled, A/Gr = air-granulated
A/Cl = air-cooled, W/Gr = water-granulated
R.K. = rotary kiln, B.F. = blast furnace
E.F. = electric furnace
FeO** = total iron

TABLE 2 - Normative Compositions of Ferro-Nickel Slags (in Weight %)

Norms	A	B	C	D	E*	F*
Olivine	8.8	23.2	18.8	18.7	14.4	6.1
Fo	7.1	20.2	17.6	15.4	12.7	5.5
Fa	1.7	3.0	1.2	3.3	1.7	0.6
	Fa_{14}	Fa_9	Fa_5	Fa_{13}	Fa_9	Fa_7
Enstatite	68.4	66.5	72.3	74.7	82.1	45.2
En	56.1	58.5	68.1	62.3	73.2	41.0
Fs	12.3	8.0	4.2	12.4	8.9	4.2
	Fs_{14}	Fs_9	Fs_5	Fs_{13}	Fs_9	Fa_7
Diopside	14.1	1.5	0.7			37.3
Wo	7.4	0.8	0.4			19.8
En	5.5	0.6	0.3			15.9
Fs	1.2	0.1				1.6
Anorthite	6.3	6.1	5.8	1.8	1.0	7.9
Chromite	1.8	1.9	1.6	1.8	1.0	0.9
Spinel				1.5	1.2	

E*, F* = currently not produced
Fo = forsterite, Fa = fayalite, Fa_{14} = molar ratio of fayalite component in olivine
En = enstatite, Fs = ferrosilite, Fs_{14} = molar ratio of ferrosilte component in pyroxene
Wo = wollastonite component

TABLE 3 - Modal Compositions of Ferro-Nickel Slags Measured by Microscopy (in Volume %)

Slag / Minerals	A av	A Au	B av	B B_S	B B_L	B B_F	C av	C C_T	C C_M	C C_B	D	E*	F*
Olivine	4.4	4.1	10.3	15.3	10.0	6.1	13.5	14.7	19.9	6.1	16.6	6.9	0.3
Pyroxene	65.7	69.6	38.6	30.7	41.3	31.5	82.3	59.6	76.7	90.5			
Protoenstatite		tr	38.6	30.7	41.3	31.5	13.7	(26)	6.7	3.7			
Clinoenstatite	0.1	1.1					68.6	(34)	70.0	86.4			
Orthoenstatite	64.4	62.7											
Pigeonite	0.1	0.4								0.4			
Augite	1.1	5.4											
Glass	29.2	24.6	51.1	54.0	48.7	62.4	4.0	25.7	3.1	3.2	83.4	93.1	99.7
Quenched Glass	5.9	2.5	1.7	1.1	2.5	9.8					6.4	52.4	99.7
Semi-Qu Glass	4.0	3.8	8.9	16.5	7.6	20.5		16.0			77.0	40.7	
pale yell. br											(17)	(22)	
yell. brown**			8.9	16.5	7.6	20.5	1.0	16.0			(60)	(19)	
brown	4.0	3.8											
Medium Glass	19.3	18.3	36.6	34.8	33.1	30.8	0.5	9.5		1.5			
Annealed Glass							2.5	0.2	3.1	1.7			
Devitrified Gl			3.9	1.6	5.5	1.3							
Others	0.7	1.7	tr	tr	tr	tr	0.2	tr	0.3	0.2	tr	0.1	tr
Chromite		0.1					0.1		0.1	0.1			

E*, F* = currently not produced, av = crushed average sample, A_U = uncrushed slag
B_S = quickly discharged slag, B_L = slowly discharged slag, B_F = fine fraction (< 2mm)
C_T, C_M, C_B = uncrushed, top, middle, bottom unit of slag flow, respectively
Semi-Qu Glass = semi-quenched glass, Devitrified Gl = devitrified glass, tr = trace
** = only a small portion of this glass (SiO_2 60%), is considered potentially reactive

TABLE 4 - EPMA Compositions of Interstitial Glasses of Ferro-Nickel Slags

Slag	Water-Granulated Slag(D)					Air-Granulated Slag(B) (Bs)				
	Fine	Medium		Coarse		Fine		Medium	Coarse	
	T291	T222	T224	T226	T294	T205	T203	T202	T215	T284
Glass	Qu	Semi-Qu	Semi-Qu	Semi-Qu	Semi-Qu	Qu	Semi-Qu	Semi-Qu	Semi-Qu	Med
Color	Color-less	Pale Yell.Br	Yell. Brown	Yell. Brown	Yell. Brown	Pale Brown	Yell. Brown	Pale Yell.Br	Yell. Brown	Yell. Brown
Dia.	0.4mm	2.1mm	>1.8mm	4.0mm		0.4mm	0.5mm	1.5mm	>>1.8mm	
Depth	0.15mm	1.05mm	1.3mm	0.15mm	0.3mm	0.1mm	0.15mm	0.2mm	-	-
Crystal	-	Ol	Ol	Ol	Ol	-	Ol	Ol	Ol	Ol+(Px)
SiO_2	52.13	53.73	56.05	58.19	60.23	53.03	55.47	59.10	61.97	65.87
TiO_2	0.05	0.03	0.07	0.06	0.12	0.06	0.07	0.05	0.14	0.24
Al_2O_3	1.84	2.28	3.21	3.61	6.50	2.60	3.83	3.40	6.25	10.04
Cr_2O_3	1.33	1.05	1.71	1.86	2.21	1.39	2.27	0.72	1.80	1.41
FeO*	9.52	7.78	12.82	14.32	11.64	6.40	6.73	6.14	6.34	7.36
MnO	0.49	0.36	0.76	0.91	0.73	0.50	0.55	0.50	0.61	0.68
MgO	33.84	33.56	24.76	19.75	17.84	33.96	28.98	28.93	19.67	9.73
CaO	0.32	0.46	0.93	0.62	0.99	0.68	0.63	1.06	1.44	2.83
Na_2O	0.01	0.03	0.02	0.03	0.05	0.00	0.20	0.07	0.17	0.26
K_2O	0.02	0.03	0.00	0.01	0.03	0.03	0.33	0.40	0.16	0.27
Total	99.55	99.31	100.33	99.36	100.34	98.65	99.06	100.37	98.55	98.69
Q	-	-	6.4	15.4	21.6	-	3.4	6.5	23.4	37.2
An	1.6	2.2	4.5	3.1	4.9	3.3	3.0	5.2	7.1	14.2

Slag	Air-Cooled Slag(C) (C_T)					Water-Cooled Slag(A) (A_U)				
	Glassy	Surface	Trans. Z	Interior		Surface	Trans. Z	Interior		
	T99	T100	T252	T246	T102	T91	T87	T70	T75	T668
Glass	Semi-Qu	Semi-Qu	Med	Ann	Ann	Qu	Semi-Qu	Med	Ann	Ann
Color	Yell. Brown	Yell. Brown	Brown	Pale Brown	Color-less	Color-less	Brown	Pale Brown	Pale Brown	Pale Brown
Depth	1mm	4mm	7mm	10mm	12mm	1mm	5mm	10mm	10mm	-
Crystal	Ol	Ol	Ol+Px	Ol+Px	Ol+Px	Ol+Px	$Ol+Px_2$	$Ol+Px_3$	$Ol+Px_3$	$Ol+Px_3$
SiO_2	61.59	64.21	64.79	64.58	58.76	54.22	53.88	54.03	55.44	55.93
TiO_2	0.06	0.18	0.25	0.27	0.34	0.09	0.09	0.18	0.14	0.10
Al_2O_3	2.38	7.09	11.01	13.25	18.62	4.33	4.24	5.73	9.64	8.68
Cr_2O_3	1.56	1.64	2.26	1.63	0.07	1.19	1.04	0.78	0.44	0.39
FeO*	6.22	6.00	9.49	8.80	8.81	10.89	13.70	13.88	12.82	14.78
MnO	0.63	0.97	1.25	1.24	1.41	0.33	0.44	0.49	0.39	0.50
MgO	27.58	17.18	8.51	5.42	2.89	16.76	13.49	11.50	5.12	5.21
CaO	0.43	1.55	2.32	3.13	5.93	10.96	12.48	13.20	13.11	12.99
Na_2O	0.11	0.19	0.38	0.61	1.07	0.13	0.12	0.13	0.40	0.38
K_2O	0.08	0.08	0.24	0.28	0.40	0.18	0.13	0.22	0.47	0.38
otal	100.64	99.09	100.50	99.21	98.30	99.08	99.64	100.15	97.97	99.33
Q	13.5	29.1	35.9	37.9	26.2	5.0	5.6	6.4	14.2	13.6
An	2.1	7.7	11.4	15.7	29.9	10.8	10.7	14.4	23.6	21.0

FeO* = total iron, Trans. Z = transitional zone
Qu = quenched glass, Semi-Qu = semi-quenched glass Med = medium glass
Ann = annealed glass, Dia. = diameter of spherical grain of slag (> = fragmented grain)
Depth = depth of analysis point from slag surface, Crystal = accompanying crystals
Ol = olivine, Px = enstatite, Px_2 = enstatite and pigeonite
Px_3 = enstatite, pigeonite and augite, Q, An = normative quartz and anorthite of glass

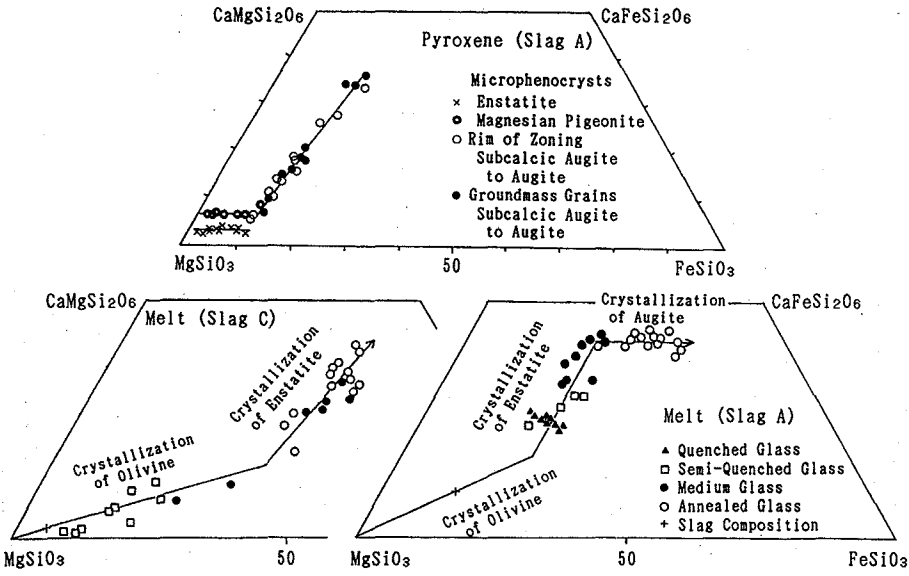

Figure 1 Compositional changes of pyroxene and melt in sintered, high-calcium, ferro-nickel slag (A), compared with molten low-calcium slag (C)

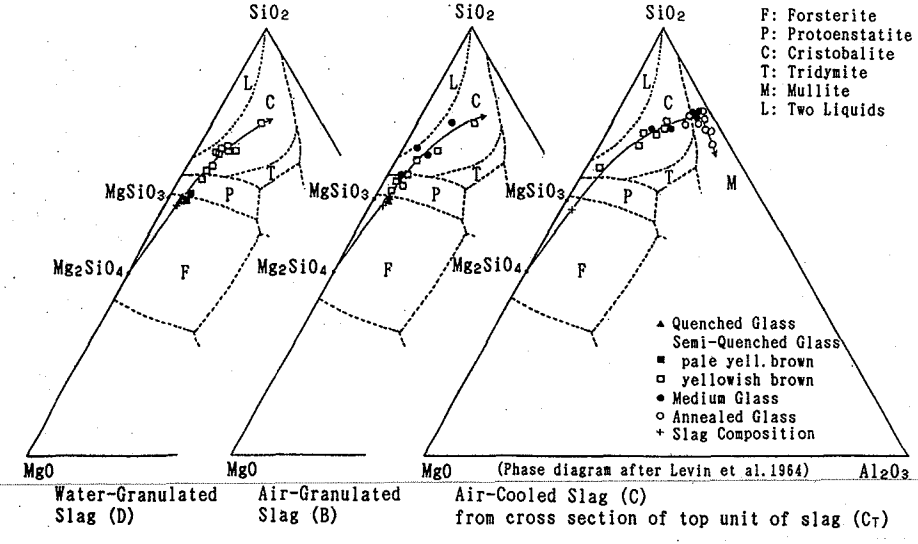

Figure 2 Compositional changes during cooling of melt in molten, low-calcium, ferro-nickel slags (B, C, D)

TABLE 5 - Texture of Ferro-Nickel Slags

Slag	Low-Calcium Molten Slag(B, C, D)			High-Ca Sinter(A)
Glass	Texture	Mineral	Cooling Rate(9)	Mineral
Quenched Glass	Glassy	Gl	>3600 °C/min	Gl Ol, En(Pg)
Semi-Qu Glass	Spinifex	Gl Ol	>300 °C/min	Gl Ol, En, Pg
Medium Glass	Radial pyroxene	Gl Ol, En	<300 °C/min	Gl, Ol, En Pg, SA
Annealed Glass	Holo-crystal	(Gl) Ol, En	<3 °C/min	(Gl)Ol, En Pg, SA-Ag
Devitrified Gl	Crypto-crystal	Gl En		

Cooling Rate, based on Matsuo et al. (9)
Semi-Qu = semi-quenched, Gl = glass
Holo crystal = holocrystalline
Ol = olivine, En = enstatite, Ag = augite
Pg = pigeonite, SA = subcalcic augite

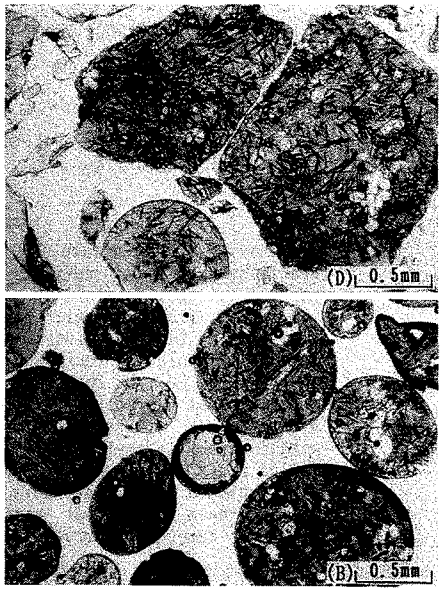

Figure 3 Spinifex texture of slag (D) and radial pyroxene texture of slag (B)

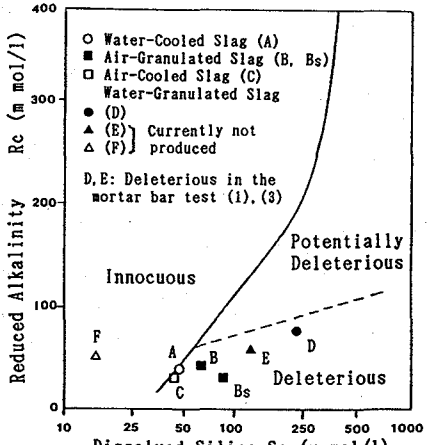

A, B, C, D: Committee (3)
Bs: Tamura et al. (11)
E, F: Yamamoto and Akiyama(1)

Figure 4 Chemical test of some Japanese ferro-nickel slags

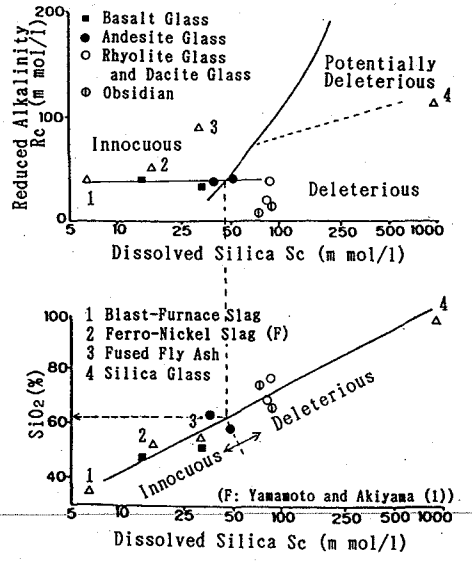

Figure 5 Chemical test of artificial and natural glasses (after Katayama et al. (16))